IEEE Access
Multidisciplinary | Rapid Review | Open Access Journal

Date of publication xxxx 00, 0000, date of current version xxxx 00, 0000.

Digital Object Identifier 10.1109/ACCESS.2022.Doi Number

Mid-course Trajectory Optimization for Short-Range Head-on Engagement via Sequential Convex Programming

Hyuck-Hoon Kwon[1], Member, IEEE, Jang-Seong Park[1], Jeong-Hun Kim[1], and Yong-su Han[1]
[1]Global PGM System Design Center, LIG Nex1, Seongnam-si, South Korea

Corresponding author: Hyuck-Hoon Kwon (e-mail: hyuckhoon.kwon@gmail.com).

ABSTRACT If an aerial defense missile with a limited strapdown field-of-view (FOV) is launched with a restricted launch angle against an incoming target at high altitude, there are significant difficulties in establishing an appropriate collision course for head-on engagement. Owing to the time-varying characteristics of the initial phase with several linear and nonlinear constraints, the analytical approach is unsuitable for obtaining the optimal solution. In this paper, a mid-course trajectory for short-range head-on engagement was generated using a convex programming approach. The time-varying characteristics of mass and velocity were considered based on the thrust profile, and the maximum flight path angle was limited as an additional constraint to prevent excessive trajectory shaping. The original nonlinear optimization problem was converted into a convex optimization problem with state augmentation, linearization, and lossless convexification. For lossless convexification, a modified optimization problem with a regularization term is suggested, and it is proved based on the maximum principal of optimal control theory. The numerical results of the modified optimization problem show that the proposed approach is effective for head-on engagement, ensuring lossless convexification. Finally, the results of the convex programming approach were compared with those of state-of-the-art nonlinear programming for verification.

INDEX TERMS Head-on Trajectory, Ground-to-Air Missiles, Lossless Convexification, Sequential Convex Programming, Short-Range Engagement

I. Introduction

In recent years, various cheap and high-performance drones have been released and used in various fields, including military applications. Accordingly, drone attacks on critical infrastructure are emerging as a major issue in countries in conflict, but there is no effective missile defense system[1]. In the case of a missile defense system for intercepting an incoming target, several studies have proposed three types of engagement scenarios: tail chase, head pursuit, and head-on[2-5]. First, tail-chase interception is possible only when the guided missile maintains a higher velocity than that of the target. However, it takes a longer time to generate a tail-chase trajectory and is unsuitable for an incoming target at high altitude because of safety issues in the case of failure. Second, in the head pursuit scenario, the guided missile predicts the target trajectory, flies in advance to the target, and then neutralizes the target in the same direction as the target. Although it is possible to cope with high-speed incoming targets when a missile is relatively slow compared to a target, the disadvantage is that accurate target information should be continuously provided by the target tracking system, such as radar or seeker, to detect and track targets coming from behind. Finally, head-on engagement is the most common scenario against aerial targets, in which the engagement time is shorter than that of tail-chase and head pursuit scenarios, and an economically effective missile with limited strapdown FOV can cope with cheap aerial targets considering the collision triangle geometry of the terminal homing phase. However, it has shortcomings in that a fast autopilot response with sufficient maneuverability is required because of the high relative velocity, and an appropriate collision course should be feasible for each

scenario. In this study, a guided missile with a strapdown seeker is considered an effective aerial defense system against various targets, owing to its economic advantage. For a missile equipped with a limited FOV of the strapdown seeker, the manner in which the head-on geometry is generated has a significant influence on the engagement result. In particular, short-range head-on engagement will be addressed to maximize the engagement area. However, it is not trivial to generate the head-on engagement area within a short range owing to the time-varying characteristics and several constraints of the initial phase. It is necessary to consider analytical or numerical approaches to control the terminal impact angle for head-on engagement.

Impact angle control algorithms have been proposed based on optimal control theory, proportional navigation guidance. Ryoo et al. proposed the energy minimization optimal guidance law to cope with the impact angle constraint as well as zero miss distance[6,7]. For the additional constraint of seeker field-of-view, Park et al. used the optimal control theory with a state variable inequality constraint consisting of three optimal phases[8]. Modification of proportional navigation guidance law is presented for impact angle control based on pure proportional navigation guidance[9], biased proportional navigation guidance[10], and switched-gain guidance[11]. Because general analytic approaches assume that the missile is a time-invariant system with specific constraints, it is difficult to expect an optimal result in a time-varying system with several constraints. On the other hand, various numerical methods might be proposed to generate the optimal trajectory in order to consider the practical constraints in a more realistic environment[12-15]. For the past decades, the nonlinear programming approach has been widely used owing to its convenience and coverage; however, it has the disadvantages of initial condition sensitivity, long computation time, and convergence issues. Recently, a variety of learning-based trajectory generation approaches have been proposed, but there are limitations in considering various constraints or engagement scenario in a realistic environment ensuring computational stability and performance[16-18]. As an alternative, convex programming approaches have been recently studied in various fields, including the aerospace field, to compensate for the disadvantages of nonlinear programming. Lu et al. proposed the conic programming approach to rendezvous and proximity operation by a lossless relaxation technique[19], and Liu et al. suggested a methodology to use second-order cone programming for nonconvex optimal control problems with concave inequality constraints and nonlinear terminal equality constraint by successive linearization[20], and it was applied to entry trajectory optimization problem[21]. Szmuk et al. also used the successive convexification to free-final-time 6-DOF power descent landing guidance[22]. Various theoretical and experimental achievements over the past 10 years have been presented in several papers[23-25].

If the original problem can be defined or transformed in a convex form, the problem can be solved effectively with polynomial time, ensuring convergence. However, because general engineering problems, including the problem considered in this study, are described as nonlinear systems, additional procedures are required to convert general nonlinear optimal control problems into convex problems. The following three problems are the main considerations of the convex programming approach. At first, the differential or integration equations are transformed into algebraic equations using an appropriate method, such as the trapezoidal or Euler rule. Second, several nonlinear constraints should be convexified using linearization or relaxation. The linearization approach is straightforward and simple to implement, but the optimality of the original problem is not guaranteed when the problem is highly nonlinear. On the other hand, the relaxation approach is a way to avoid the nonconvex problem, but the relaxed problem might be quite different from the original one. If we can prove that the relaxation does not affect the solution of the original problem, the nonconvex constraints can be relaxed while generating the same results as the original problem. This is known as lossless convexification[26-34]. Finally, an independent variable with a monotone property should be defined for specific initial and final values. For free final time problems, flight time should be sequentially predicted or other states such as downrange or altitude should be set as independent variables[31-34].

In this paper, the mid-course trajectory for short-range head-on engagement was generated using a convex programming approach. Assuming that a missile is launched at a specific launch angle against an incoming target at a short range and high altitude, we attempt to determine the minimum final flight path angle for head-on engagement. The maximum flight path angle limit was additionally set to prevent excessive trajectory shaping with increased flight time. The mass and velocity of the guided missile change with flight time according to the thrust profile, and the missile acceleration is limited in conjunction with the missile velocity and maximum angle of attack. In summary, the original problem considered in this paper is a nonlinear optimal control problem with nonlinear dynamics, flight path angle, angle-of-attack constraint, and free final time. It is converted to a convex optimization problem using the linearization of the dynamic equation and nonlinear constraint, lossless convexification, and state augmentation of the flight time with proper discretization. In particular, for lossless convexification, the original problem is modified using the regularization term of the final velocity, and the lossless convexification of the modified problem is proved

based on the maximum principle of optimal control theory. The main contributions of this paper are as follows. The problem is defined as a mid-course trajectory optimization problem to maximize the engagement area. First, the problem to maximize the engagement area for aerial defense system is defined as a mid-course trajectory optimization problem based on head-on scenario. Second, lossless convexification for convergence is proven based on the regularization term additionally applied to the originally defined problem. Lastly, the numerical results of the proposed modified problem are compared to the analytical results of impact angle control and numerical results of nonlinear programming to show the superior results and effectiveness of the proposed approach.

This paper is organized as follows. Section 2 provides a summary of the midcourse trajectory optimization problem formulation with state augmentation. In Section 3, direct transcription, including linearization and discretization, is described in detail. In Section 4, a modified problem is proposed, and lossless convexification is proved using optimal control theory. In Section 5, the numerical results of sequential convex programming are presented and compared to the results of the analytical and nonlinear programming approaches. Finally, the conclusions are presented in Section 6.

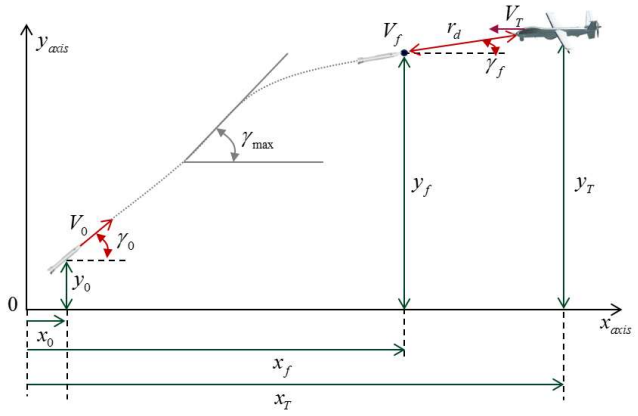

FIGURE 1. Mid-course Trajectory Geometry.

II. Problem Description

In this section, the mid-course trajectory optimization problem for short-range head-on engagement is defined. Figure 1 shows the trajectory from the launch point to the target detection point with the flight path angle and terminal range constraints. The flight path angle constraint is set to prevent excessive trajectory shaping and to engage faster in a safe area, and the terminal range constraint is set for the transition to the terminal phase at the distance of the target detection range of the seeker. The flight phase of a missile equipped with a solid propulsion system consists of a boost phase and glide phase based on the burning time, and the flight trajectory should consider both phases. The subscripts 0, f, and T indicate the initial, final, and target states, respectively, in Figure 1. Consider the nonlinear equations of motion in the two-dimensional longitudinal plane in Eq. (1) ~ Eq. (4)

$$\dot{x} = V cos\gamma \tag{1}$$

$$\dot{y} = V sin\gamma \tag{2}$$

$$\dot{V} = \frac{1}{m}(T cos\alpha - D) - g sin\gamma \tag{3}$$

$$\dot{\gamma} = \frac{1}{mV}(T sin\alpha + L) - \frac{1}{V} g cos\gamma \tag{4}$$

where

$$T = \begin{cases} T_0 & t \le t_{thr} \\ 0 & t > t_{thr} \end{cases} \tag{5}$$

$$m = \begin{cases} m_0 - \frac{m_{thr}}{t_{thr}} t & t \le t_{thr} \\ m_0 - m_{thr} & t > t_{thr} \end{cases} \tag{6}$$

$$L = \left(\frac{1}{2}\rho V^2 S_{ref}\right) \cdot \left(C_{L_\alpha}\alpha\right) \tag{7}$$

$$D = \left(\frac{1}{2}\rho V^2 S_{ref}\right) \cdot \left(C_{D_0} + C_{D_\alpha}\alpha^2\right) \tag{8}$$

where x, y, V, γ represent the downrange, altitude, velocity, and flight-path angle of the missile, respectively. And m is the missile mass, g is the gravitational constant, and T is the thrust magnitude with thrust mass m_{thr} and burning time t_{thr}. L and D indicate the aerodynamic lift and drag forces, respectively, and are described in Eq. (7) and Eq. (8) in a simple form: ρ, S_{ref} represent the air density and reference area, respectively, and $C_{L_\alpha}, C_{D_0}, C_{D_\alpha}$ are the aerodynamic coefficients of lift and drag, respectively.

A. Optimization Problem

For head-on engagement, the flight path angle during the transition from the mid-course phase to the terminal phase should be as small as possible against a level-flying target. This assumption holds true because typical long-range drones glide steadily for a high lift-to-drag ratio without maneuvering. Thus, the main objective of our system is to make the flight-path angle at transition as close to 0deg as possible. In addition, during the entire flight regime, the angle of attack for short-range tactical missiles was assumed to be small to ensure stability of the time-varying system. Therefore, the sinusoidal functions can be simplified as shown in Eq. (9) through the small-angle approximation:

$$cos\alpha \approx 1, sin\alpha \approx \alpha \tag{9}$$

If the downrange, altitude, velocity, and flight path angle are selected as the state variables of the missile and the angle of attack and its square are selected as the control variables, the

nonlinear dynamic equations of the missile are described as follows:

$$\dot{p} = f(p) + B(p)u = \begin{bmatrix} V\cos\gamma \\ V\sin\gamma \\ \frac{T}{m} - g\sin - \frac{\rho V^2 S_{ref}}{2m} C_{D_0} \\ -\frac{1}{V} g\cos\gamma \end{bmatrix} + \begin{bmatrix} 0 & 0 \\ 0 & 0 \\ 0 & -\frac{\rho V^2 S_{ref}}{2m} C_{D_\alpha} \\ \frac{1}{mV}\left(T + \frac{\rho V^2 S_{ref}}{2} C_{L_\alpha}\right) & 0 \end{bmatrix} u \quad (10)$$

where Eq. (5), Eq. (6), and

$$p = [x \quad y \quad V \quad \gamma]^T \quad (11)$$

$$u = [\alpha \quad \alpha^2]^T \quad (12)$$

where ṗ represents the derivatives of the state variable p with respect to time t. Within the limited engagement geometry, an excessively curved trajectory may be generated even behind the launch point. The constraint on the flight-path angle in Eq. (13) is set for a safe and fast engagement.

$$\gamma \le \gamma_{max} \quad (13)$$

Because the square of the angle of attack is selected as the second input variable in Eq. (10) for the control-affine system, the first and second input variables have a direct relationship. In addition, because the acceleration limit of a guided missile is directly related to the angle of attack, the angle of attack limit is set to α_{max} as follows:

$$u_1^2 = u_2 \quad (14)$$

$$0 \le u_2 \le u_{max}(= \alpha_{max}^2) \quad (15)$$

The mid-course phase of the guided missiles is converted to the terminal phase after a seeker detects and tracks a target. Although the seeker's detection range generally varies depending on the environmental conditions, target size and shape, and detection algorithm, it is assumed to be constant for the design of the guidance algorithm. Therefore, the final condition of the mid-course phase is expressed by Eq. (16) and (17), respectively.

$$x(t_f) = x_T - r_d \cos\gamma(t_f) \quad (16)$$

$$y(t_f) = y_T - r_d \sin\gamma(t_f) \quad (17)$$

Combining the dynamic equation and constraints described above, the original optimal control problem P0 can be defined as follows:

- P0 : $\min J = \gamma(t_f)$
  - dynamics : $\dot{p} = f(p) + B(p)u$
  - state constraint: $\gamma(t) \le \gamma_{max}$
  - control constraint : $u_1^2 = u_2, 0 \le u_2 \le u_{max}$
  - initial condition: $p(t_0) = [x(t_0), y(t_0), V(t_0), \gamma(t_0)]^T$
  - final condition : $x(t_f) = x_T - r_d \cos\gamma(t_f)$, $y(t_f) = y_T - r_d \sin\gamma(t_f)$

B. State Augmentation

To solve the optimization problem numerically, an independent variable with monotonic property and specific boundary values is required. In the P0 optimization problem, it is difficult to set an independent variable such as downrange or altitude, because the final boundary values are not determined owing to the terminal constraint. Therefore, in this paper, the normalized flight time from launch to the end of the mid-course phase was set to an additional state as follows:

$$\tau = (t - t_0)/\beta \quad (18)$$

$$d\tau = dt/\beta \quad (19)$$

where β is defined as the flight time from launch(t_0) to the end of the mid-course phase(t_f). If β is added to a new state variable and is also used as an independent variable, the nonlinear dynamic equation of the missile is transformed as follows:

$$q' = \frac{dq}{d\tau} = f_q(q) + B_q(q)u = \beta \begin{bmatrix} V\cos\gamma \\ V\sin\gamma \\ \frac{T}{m} - g\sin - \frac{\rho V^2 S_{ref}}{2m} C_{D_0} \\ -\frac{1}{V} g\cos\gamma \\ 0 \end{bmatrix} +$$

$$\beta\begin{bmatrix} 0 & 0 \\ 0 & 0 \\ 0 & 0 \\ \frac{1}{mV}\left(T+\frac{\rho V^2 S_{ref}}{2}C_{L_\alpha}\right) & -\frac{\rho V^2 S_{ref}}{2m}C_{D_\alpha} \\ 0 & 0 \end{bmatrix} u \tag{20}$$

where Eq. (5), Eq. (6), Eq. (12), and

$$q = [x \quad y \quad V \quad \gamma \quad \beta]^T \tag{21}$$

where q′ represents the derivatives of the state variable q with respect to dimensionless time τ. Based on the newly defined state and independent variables, the original problem P0 can be described as problem P1.

- P1 : $\min J = \gamma(\tau_f)$
  - dynamics : $q' = f_q(q) + B_q(q)u$
  - state constraint : $\gamma(\tau) \le \gamma_{max}$
  - control constraint : $u_1^2 = u_2, 0 \le u_2 \le u_{max}$
  - initial condition :

$$q(\tau_0) = [x(\tau_0), y(\tau_0), V(\tau_0), \gamma(\tau_0), \beta(\tau_0)]^T$$

  - final condition: $x(\tau_f) = x_T - r_d \cos\gamma(\tau_f)$

$$y(\tau_f) = y_T - r_d \sin\gamma(\tau_f)$$

III. Direct Transcription of Optimization Problem

For the numerical approach to the P1 optimization problem, the remedies for the nonlinear dynamic equation and terminal constraints should be presented. First, the nonlinear equation and terminal constraints were convexified through linearization with the trust region. Second, continuous-time dynamic equations are converted into a discrete equivalent based on a trapezoidal rule with equal intervals. The phase transition from boost to glide will be carefully considered in the interval where the burning of solid propulsion ends.

A. Linearization of Dynamics Equation

The nonlinear dynamic equations in Eq. (20) are linearized based on the partial linearization method, which is different from the conventional linearization method in that it only linearizes the state part $f_q(q)$, not the control part $B_q(q)$. This has the advantage of reducing undesirable oscillations in the control profiles during the optimization process[21]. Assuming that the optimal solution in k-th iteration is q^k, the partial-linearized system of Eq. (20) is obtained asfollows:

$$q' = A(q^k)q + B_q(q^k)u + c(q^k) \tag{22}$$

where

$$A(q^k) = \frac{\partial f_q(q^k)}{\partial q} = \begin{bmatrix} 0 & 0 & a_{13} & a_{14} & a_{15} \\ 0 & 0 & a_{23} & a_{24} & a_{25} \\ 0 & 0 & a_{33} & a_{34} & a_{35} \\ 0 & 0 & a_{43} & a_{44} & a_{45} \\ 0 & 0 & 0 & 0 & 0 \end{bmatrix} \tag{23}$$

$$a_{13} = \beta^k cos\gamma^k$$
$$a_{14} = -\beta^k V^k sin\gamma^k$$
$$a_{15} = V^k cos\gamma^k$$
$$a_{23} = \beta^k sin\gamma^k$$
$$a_{24} = \beta^k V^k cos\gamma^k$$
$$a_{25} = V^k sin\gamma^k$$
$$a_{33} = -\beta^k \rho V^k S_{ref} C_{D_0}/(2m)$$
$$a_{34} = -\beta^k g cos\gamma^k$$
$$a_{35} = T/m - g sin\gamma^k - \rho(V^k)^2 S_{ref} C_{D_0}/(2m)$$
$$a_{43} = \beta^k g cos\gamma^k/(V^k)^2$$
$$a_{44} = \beta^k g sin\gamma^k/V^k$$
$$a_{45} = -g cos\gamma^k/V^k$$
$$c(q^k) = f_q(q^k) - A(q^k)q^k \tag{24}$$

Because linearization cannot preserve the actual nonlinear characteristics as they deviate from the reference point, the following trust region is required for the validity of linearization.

$$|q - q^k| \le r_q \tag{25}$$

where r_q is a constant and the inequality corresponds to each element of the states individually.

B. Linearization of Terminal Constraint

Because the terminal constraints in Eq. (16) and Eq. (17) are nonlinear equality equations, we must linearize them to formulate a convex problem. In this paper, we proceeded with two stages of linearization to obtain more accurate results, as proposed in Ref. [20]. First, we define the nonlinear terminal constraint as:

$$h(q^k) = \begin{bmatrix} x^k(\tau_f) - \left(x_T - r_d cos\gamma^k(\tau_f)\right) \\ y^k(\tau_f) - \left(y_T - r_d sin\gamma^k(\tau_f)\right) \end{bmatrix} = 0 \tag{26}$$

In the first-stage linearization process, the second- or higher-order terms are ignored, and the first-order linearization results are only used for optimization, as shown in Eq. (27).

$$h(q^k) + D(q^k)(q - q^k) = 0 \tag{27}$$

where

$$D(q^k) = \begin{bmatrix} 1 & 0 & 0 & -r_d sin\gamma^k(\tau_f) & 0 \\ 0 & 1 & 0 & r_d cos\gamma^k(\tau_f) & 0 \end{bmatrix} = 0 \tag{28}$$

Let us define q_{k1} as the optimization result using first-stage linearization. In the second-stage linearization, the second-order term of the terminal constraint is estimated, and the optimization process is repeated based on the results of the first-stage result.

$$h(q^k) + D(q^k)(q - q^k) + h_c(q_{k1}) = 0 \tag{29}$$

where $h_c(q_{k1}) = h(q_{k1}) - h(q^k) - D(q^k)(q_{k1} - q^k)$

The final result obtained by the two stages of linearization is updated to q^{k+1}. This approach can consider the second-order term of the Taylor series even without calculating the Hessian matrix.

C. Discretization of Dynamic Equation

Because the dynamic equation is described as a continuous differential equation, it should be converted into an algebraic form using an appropriate integration technique. In this paper, the trapezoidal technique, which is widely used in optimization, was applied for discretization[31,32].

$$q_i^k = q_{i-1}^k + (\Delta\tau/2)\left[f_q(q_{i-1}^k) + B_q(q_{i-1}^k)u_{i-1}^k\right] + (\Delta\tau/2)\left[f_q(q_{i-1}^k) + B_q(q_{i-1}^k)u_{i-1}^k\right], \quad i = 1, \dots, N \tag{30}$$

where $\Delta\tau(= 1/N)$ means the interval obtained from equivalent N sections. In addition, because the missile has a specific burning time, t_{thr} in Eq. (5), it is necessary to identify the interval that includes the burning time and appropriately reflect this in the equation. The i_T-th interval, which includes the burning time t_{thr} can be determined based on the estimated total flight time β as in Eq. (31). Accordingly, the appropriate equation at interval was calculated using Eq. (32).

$$(i_T - 1)/N \le (t_{thr}/\beta) \le (i_T/N) \tag{31}$$

$$q_{i_T}^k = q_{i_T-1}^k + \delta_1\Delta\tau\left[f_q(q_{i-1}^k) + B_q(q_{i-1}^k)u_{i-1}^k\right] + \delta_2\Delta\tau\left[f_q(q_{i-1}^k) + B_q(q_{i-1}^k)u_{i-1}^k\right], \quad i = 1, \dots, N \tag{32}$$

$$where\ \delta_1 = i_T - N(t_{thr}/\beta), \delta_2 = 1 - \delta_1$$

Assuming that the mass of the missile decreases uniformly with time during the boost phase, the mass profile can be described using Eq. (31).

$$m_i^k = \begin{cases} m_0 - m_{thr}\left(i \times \frac{\beta}{N \cdot t_{thr}}\right) & i \le i_{thr} \\ m_0 - m_{thr} & i > i_{thr} \end{cases} \tag{33}$$

Reflecting on the linearization and discretization results of the dynamic equation and the constraints mentioned above, the following optimization problem P2 can be defined:

- P2 : $\min J = \gamma(\tau_N)$
  - dynamics : $M\bar{q} = F$
  - state constraint: $\gamma(\tau_i) \le \gamma_{max}, \quad i = 0{:}N$
    $|q - q^k| \le \varepsilon_q$
  - control constraint : $u_1^2(\tau_i) = u_2(\tau_i), 0 \le u_2(\tau_i) \le u_{max}$
  - initial condition :
    $q(\tau_0) = [x(\tau_0), y(\tau_0), V(\tau_0), \gamma(\tau_0), \beta(\tau_0)]^T$
  - final condition: $h(q^k) + D(q^k)(q - q^k) + h_c(q_{k1}) = 0$

IV. Lossless Convexification

In the case of the P2 optimization problem, the relationship between the two input variables is described in the control constraints, which is a non-convex constraint. If an equal sign is replaced with an inequality sign, the problem can be converted into a convex form and the optimization results can be easily solved. If the result of the relaxed optimization problem using the inequality sign is the same as that of the original optimization problem, it is called lossless convexification or exact convex relaxation. To date, lossless convexification has been demonstrated and used in various types of problems based on proof using the maximum principle of optimal control theory. In this section, we suggest lossless convexification related to the control constraint in the P2 optimization problem.

A. Application to Optimal Control Theory

Optimal control problems with state constraints have been proven using the maximum principle[29-33]. First, the trust region owing to linearization should be sufficiently large so that it does not apply as an additional barrier for the proof. This is reasonable in problems where nonlinearity is not significant and will be checked through simulation results in Section V. Accordingly, the Hamiltonian, Lagrangian, and endpoint functions of the P2 optimization problem are defined as follows:

$$H(\tau) = p_x(a_{13}V + a_{14}\gamma + a_{15}\beta + c_1) + p_y(a_{23}V + a_{24}\gamma + a_{25}\beta + c_2)$$

$$+p_V(a_{33}V + a_{34}\gamma + a_{35}\beta + c_3 + b_{32}u_2)$$
$$+p_\gamma(a_{43}V + a_{44}\gamma + a_{45}\beta + c_4 + b_{41}u_1) \quad (34)$$

$$L(\tau) = H + \lambda_0(u_1^2 - u_2) + \lambda_1(-u_2) + \lambda_2(u_2 - u_{max}) + \nu_\gamma(\gamma - \gamma_{max}) \quad (35)$$

$$G(\tau_f) = p_0\left(\gamma(\tau_f)\right) + \xi_x(x(\tau_f) + d_{14}\gamma(\tau_f) + h_{cx}) + \xi_y(x(\tau_f) + d_{24}\gamma(\tau_f) + h_{cy}) + \xi_\gamma(\gamma(\tau_f) - \gamma_{max}) \quad (36)$$

where p_x, p_y, p_V, p_γ are the costate variables for each state, and $\lambda_0, \lambda_1, \lambda_2, \nu_\gamma, \xi_x, \xi_y, \xi_\gamma$ are Lagrangian multipliers for the control constraints, state constraint, and final conditions, respectively. And a_{ij} and b_{ij} are the elements of the i-th row and j-th column in A and B_q matrices, respectively, and c_i are the elements of the i-th row in c vector in Eq. (22). In addition, d_{ij} is the element of the i-th row and j-th column in D matrix in Eq. (28), and h_{cx}, h_{cy} are residual terms of x and y constraints due to linearization of the final condition, as in Eq. (29). Based on the maximum principle in the Appendix, the differential equations for the costate variable are represented as follows:

$$\dot{p}_x = -\partial_x L(\tau) = 0 \quad (37)$$
$$\dot{p}_y = -\partial_y L(\tau) = 0 \quad (38)$$
$$\dot{p}_V = -\partial_V L(\tau) = -\left(p_x a_{13} + p_y a_{23} + p_V a_{33} + p_\gamma a_{43}\right) \quad (39)$$
$$\dot{p}_\gamma = -\partial_\gamma L(\tau) = -\left(p_x a_{14} + p_y a_{24} + p_V a_{34} + p_\gamma a_{44}\right) \quad (40)$$
$$\dot{p}_\beta = -\partial_\beta L(\tau) = -\left(p_x a_{15} + p_y a_{25} + p_V a_{35} + p_\gamma a_{45}\right) \quad (41)$$

The stationary equations are described as follows.

$$\partial_{u_1} L(\tau) = p_\gamma b_{41} + 2\lambda_0 u_1 = 0 \quad (42)$$
$$\partial_{u_2} L(\tau) = p_V b_{32} - \lambda_0 - \lambda_1 + \lambda_2 = 0 \quad (43)$$

The complementary slackness conditions for the state and control variables are shown as follows.

$$\lambda_0 \le 0, \ \lambda_0(u_1^2 - u_2) = 0 \quad (44)$$
$$\lambda_1 \le 0, \ \lambda_1(-u_2) = 0 \quad (45)$$
$$\lambda_2 \le 0, \ \lambda_2(u_2 - u_{max}) = 0 \quad (46)$$
$$\nu_\gamma \le 0, \ \nu_\gamma(\gamma - \gamma_{max}) = 0 \quad (47)$$
$$\xi_\gamma \le 0, \ \xi_\gamma\left(\gamma(\tau_f) - \gamma_{max}\right) = 0 \quad (48)$$

The transversality conditions appears as follows

$$p_x(\tau_f) = \partial_x G(\tau_f) = \xi_x \quad (49)$$
$$p_y(\tau_f) = \partial_y G(\tau_f) = \xi_y \quad (50)$$
$$p_V(\tau_f) = \partial_V G(\tau_f) = 0 \quad (51)$$
$$p_\gamma(\tau_f) = \partial_\gamma G(\tau_f) = p_0 + \xi_x d_{14} + \xi_y d_{24} + \xi_\gamma \quad (52)$$
$$p_\beta(\tau_f) = \partial_\beta G(\tau_f) = 0 \quad (53)$$

B. Approach to Lossless Convexfication

Proof by contradiction is used to approach lossless convexification. Let us assume that there exists a certain interval $[\tau_1, \tau_2] \subset [\tau_0, \tau_f]$ that satisfies $u_1^2 < u_2$. There should exist a constant $p_0 \le 0$ for an optimal solution (q^*, u^*) that satisfies the conditions of the maximum principle.

(i) Based on this assumption, the following conditions are satisfied in the intervals $[\tau_1, \tau_2]$.

$$u_1^2 < u_2, \ u_2 > 0 \quad (54)$$

The Lagrange multipliers λ_0 and λ_1 can be determined from the complementary slackness conditions in Eq. (44) and Eq. (45).

$$\lambda_0 = \lambda_1 = 0 \quad (55)$$

(ii) From the stationary condition of u_1,.

$$\partial_{u_1} L(\tau) = p_\gamma b_{41} + 2\lambda_0 u_1 = p_\gamma b_{41} = p_\gamma\left(\frac{\beta}{mV}\left(T + \frac{\rho V^2 S_{ref}}{2} C_{L_\alpha}\right)\right) = 0 \quad (56)$$

Because T is greater than or equal to 0 and $\rho, S_{ref}, m, C_{L_\alpha}, \beta$ are generally positive,

$$p_\gamma = 0 \quad (57)$$

(iii) From the stationary condition of u_2,.

$$\partial_{u_2} L(\tau) = p_V b_{32} - \lambda_0 - \lambda_1 + \lambda_2$$

$$= p_V b_{32} + \lambda_2 = 0 \quad (58)$$

As λ_2 is less than or equal to 0, $p_V b_{32}$ should be greater than or equal to zero. The control variable parts in the Hamiltonian of Eq. (34) is derived as follows:

$$H^u(\tau) = p_\gamma b_{41} u_1 + p_V b_{32} u_2 \quad (59)$$

Based on the pointwise maximum condition, u_2 in Eq. (59) was determined according to the switching function $p_V b_{32}$.

$$u_2 \in [0, u_{max}] \quad if \quad p_V b_{32} = 0 \quad (60)$$

$$u_2 = 0 \quad if \quad p_V b_{32} > 0 \quad (61)$$

From Eq. (54), u_2 should be positive, and p_V can be calculated as follows under the condition of $b_{32} < 0$.

$$p_V = 0 \quad (62)$$

(iv) Using $p_V = p_\gamma = 0$ in Eq. (57) and Eq. (62), the differential equations in Eq. (37) to Eq. (40) can be expressed as follows:

$$p_x = l_x \quad (63)$$

$$p_y = l_y \quad (64)$$

$$p_x a_{13} + p_y a_{23} = l_x \beta cos\gamma + l_y \beta sin\gamma = 0 \quad (65)$$

$$p_x a_{14} + p_y a_{24} = -l_x \beta V sin\gamma + l_y \beta V cos\gamma = 0 \quad (66)$$

where l_x and l_y indicate constant values. By manipulation of Eq. (65) and Eq. (66),

$$\left(l_x \beta cos\gamma + l_y \beta sin\gamma\right) V sin\gamma + \left(-l_x \beta V sin\gamma + l_y \beta V cos\gamma\right) cos\gamma = l_y \beta V = 0 \quad (67)$$

$$\left(l_x \beta cos\gamma + l_y \beta sin\gamma\right) V cos\gamma - \left(-l_x \beta V sin\gamma + l_y \beta V cos\gamma\right) sin\gamma = l_x \beta V = 0 \quad (68)$$

Because β and V are positive under normal circumstance, l_x and l_y should be zero. Therefore, p_x and p_y were zero in Eq. (63) and Eq. (64).

$$p_x = p_y = 0 \quad (69)$$

According to Eq. (41) with Eq. (53), Eq. (57), Eq. (62), and Eq. (69), p_β is a constant, and its final value must be zero; therefore, it should be zero, as follows:

$$p_\beta = 0 \quad (70)$$

(v) Combining Eq. (57) and Eq. (69) with Eq. (49), Eq. (50) and Eq. (52),

$$\xi_x = \xi_y = 0 \quad (71)$$

$$p_0 + \xi_x d_{14} + \xi_y d_{24} + \xi_\gamma = p_0 + \xi_\gamma = 0 \quad (72)$$

(vi) The flight-path angle constraint is described as follows:

$$S(q) = \gamma - \gamma_{max} \leq 0 \quad (73)$$

The constraint $S(q)$ is a first-order constraint with respect to the control, and then the derivatives of the constraint are calculated.

$$\frac{dS(q)}{dq} = [0 \quad 0 \quad 0 \quad 1 \quad 0]^T \quad (74)$$

$$S(q)' = \gamma' = -\frac{\beta}{V} g cos\gamma + \frac{\beta}{mV}\left(T + \frac{\rho V^2 S_{ref}}{2} C_{L_\alpha}\right) u_1 \quad (75)$$

Then,

$$\begin{bmatrix} p_x(\tau_1^-) \\ p_y(\tau_1^-) \\ p_V(\tau_1^-) \\ p_\gamma(\tau_1^-) \\ p_\beta(\tau_1^-) \end{bmatrix} = \begin{bmatrix} p_x(\tau_1^+) \\ p_y(\tau_1^+) \\ p_V(\tau_1^+) \\ p_\gamma(\tau_1^+) \\ p_\beta(\tau_1^+) \end{bmatrix} + \eta(\tau_1) \begin{bmatrix} 0 \\ 0 \\ 0 \\ 1 \\ 0 \end{bmatrix} \quad (76)$$

Because p_γ is zero at all intervals in Eq. (57), $\eta(\tau_1)$ should be zero.

$$\eta(\tau_1) = 0 \quad (77)$$

(vii) Because the Hamiltonian, endpoint, and state constraint functions are autonomous,

$$H(t) = 0 \qquad \forall t \quad (78)$$

Summarizing the above results in this section, except for p_0 and ξ_γ, all other values of the costate, Lagrangian multiplier, and junction point vector are zero. In the next section, we

propose a modified problem to overcome the last hurdle for lossless convexification.

C. Modified Problem Proposal

For lossless convexfication, the regularization term $-c_V V(\tau_N)$, which is relatively small compared to the value of $\gamma(\tau_N)$, is added to the objective function as in optimization problem P3. This maximizes the terminal velocity, which can be adjusted according to the value of c_V.

- P3 : $\min J = \gamma(\tau_N) - c_V V(\tau_N)$
  - dynamics : $M\bar{q} = F$
  - state constraint: $\gamma(\tau_i) \le \gamma_{max}, \quad i = 0{:}N$
  - control constraint : $u_1^2(\tau_i) = u_2(\tau_i), 0 \le u_2(\tau_i) \le u_{max}$
  - initial condition :
    $$q(\tau_0) = [x(\tau_0), y(\tau_0), V(\tau_0), \gamma(\tau_0), \beta(\tau_0)]^T$$
  - final condition: $h(q^k) + D(q^k)(q - q^k) + h_c(q_{k1}) = 0$

When the objective function is adjusted, the endpoint function in Eq. (36) is converted as follows, whereas the Hamiltonian of Eq. (34), and the Lagrangian of Eq. (35) remains the same.

$$\begin{aligned} G(\tau_f) = p_0 \left(\gamma(\tau_f) - c_V V(\tau_N)\right) \\ +\xi_x\left(x(\tau_f) + d_{14}\gamma(\tau_f) + h_{cx}\right) \\ +\xi_y\left(x(\tau_f) + d_{24}\gamma(\tau_f) + h_{cy}\right) \\ +\xi_\gamma\left(\gamma(\tau_f) - \gamma_{max}\right) \end{aligned} \tag{79}$$

Based on Eq. (71) and Eq. (79), the transversality conditions in Eq. (51) and Eq. (52) are converted as follows:

$$p_V(\tau_f) = \partial_V G(\tau_f) = -c_V p_0 \tag{80}$$

$$p_\gamma(\tau_f) = \partial_\gamma G(\tau_f) = p_0 + \xi_\gamma \tag{81}$$

From the Eq. (57), Eq. (62), and Eq. (78), p_0 and ξ_γ should be zero, which is not determined in the original problem. Summarizing the above results, the following conclusions can be drawn.

$$(p_0, p(\tau), \lambda(\tau), \nu(\tau), \xi, \eta(\tau_1), \dots) = 0, \qquad \forall\tau \tag{82}$$

This contradicts the non-triviality condition (A.4) in the maximum principle of the Appendix. Therefore, the following equation holds:

$$u_1^2(\tau) = u_2(\tau), \qquad a.e. \ \ \tau \in [\tau_0, \tau_f] \tag{83}$$

Following the proof of lossless convexification, the optimization problem P3 is relaxed exactly as the following optimization problem P4.

- P4 : $\min J = \gamma(\tau_N) - c_V V(\tau_N)$
  - dynamics : $M\bar{q} = F$
  - state constraint: $\gamma(\tau_i) \le \gamma_{max}, \quad i = 0{:}N$
  - control constraint : $u_1^2(\tau_i) \le u_2(\tau_i), 0 \le u_2(\tau_i) \le u_{max}$
  - initial condition :
    $$q(\tau_0) = [x(\tau_0), y(\tau_0), V(\tau_0), \gamma(\tau_0), \beta(\tau_0)]^T$$
  - final condition: $h(q^k) + D(q^k)(q - q^k) + h_c(q_{k1}) = 0$

V. Simulation Results

In this section, a mid-course trajectory optimization for ground-to-air missiles satisfying the flight-path angle constraint was generated using sequential convex programming. The following table lists the specifications of the missile used in the numerical simulation.

TABLE I
SPECIFICATION OF GROUND-TO-AIR MISSILE

Parameter	Specification
Missile Weight	30 kg
Propellant Weight	8kg
Thrust	6000 N
Burning Time	3.0 sec
Seeker Detection Range	1.0 km
Max. Flight Path Angle	80 deg
Max. Angle-of-Attack	10 deg

The initial condition of missile is set to be as follows :

$$q(\tau_0) = [0m, 0m, 20m/s, 50deg, 20sec]^T \tag{84}$$

The distance and altitude of the target were 2km and 4 km, respectively. Therefore, the gravitational acceleration is

considered as a constant since the variation of gravitational acceleration with respect to altitude is trivial. The discrete section was set to 400, which means that the corresponding discrete points were 401, including the initial point. The trust region and convergence condition were set as follows:

$$r_q = [5km, 5km, 1km/s, 50deg, 30sec]^T \quad (85)$$

$$\varepsilon_q = [1m, 1m, 0.5m/s, 0.1deg, 0.1sec]^T \quad (86)$$

The trust region is sufficiently large considering the feasible range of each variable and the assumption of lossless convexification. The convergence condition was set to be small, based on the computation time and convergence stability within 20 iterations. The initial profile of each state and the control were set as lines connecting the initial and final conditions. All the simulations were run using MOSEK, which is state-of-the-art interior point methods, on a desktop with an Intel i5-6400 CPU with a clock-frequency of 2.7GHz and 16GB RAM.

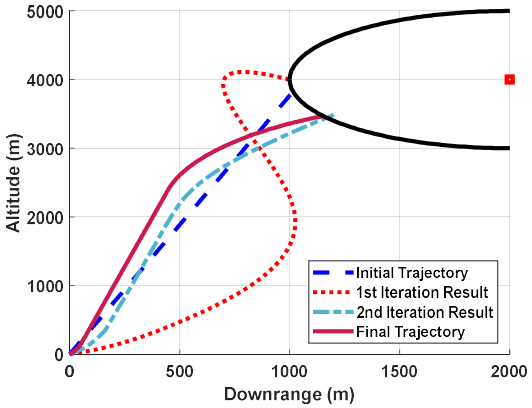

FIGURE 2. Sequential Convergence of Flight Trajectory on P4 problem with $c_V = 0.0015$

A. Verification of Lossless Convexification

In this section, the convergence results of sequential convex programming and validity of the modified problem proposal are presented.

a) Sequential convex programming results with $c_V = 0.0015$

From Figure 2, it can be observed that the converged trajectory is obtained after 7 iterations, even though the initial trajectory and the trajectory after the first iteration are significantly different from the final trajectory. This indicates that the converged result can be quickly obtained even if the initial guess is significantly different from the final value, which is one of the main advantages of convex programming. Figure 3 and 4 represent the convergence of the velocity, flight path angle, respectively. Similar to the flight trajectory, even if the initial value is very inaccurate, it can be seen that converged results are quickly obtained. In the case of velocity, an appropriate profile is obtained by reflecting the thrust profile. The constraint of the flight path angle is satisfied in all iterations, and the final value of the flight path angle is calculated to be approximately 32°.

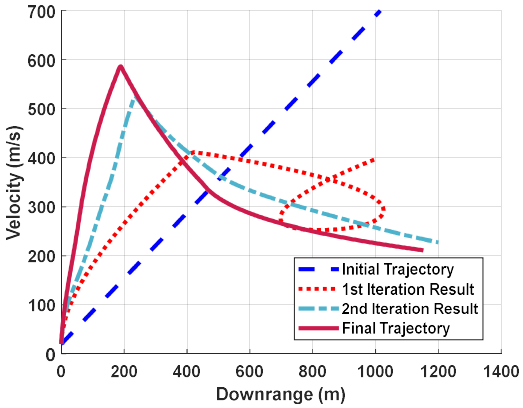

FIGURE 3. Sequential Convergence of Velocity on P4 problem with $c_V = 0.0015$

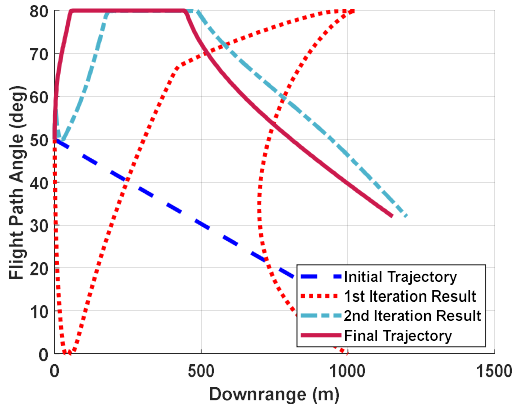

FIGURE 4. Sequential Convergence of Flight Path Angle on P4 problem with $c_V = 0.0015$

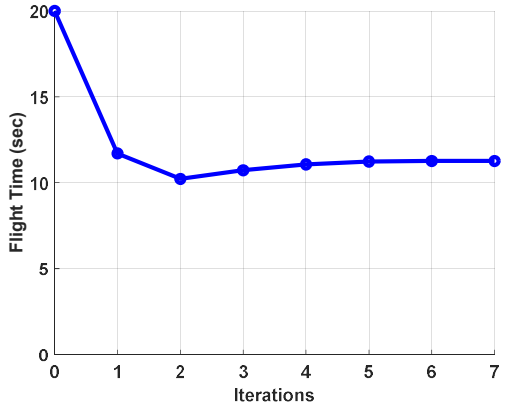

FIGURE 5. Sequential Convergence of Flight Time on P4 problem with $c_V = 0.0015$

Figure 5 shows the sequential convergence of flight time. For flight time, the initial guess was set to be 20sec. However, it can be seen that as the iteration progresses, it converges to a certain value. The residual function E is defined as in Eq. (87) to check the quantitative convergence of the proposed sequential algorithm. It represents errors of trapezoidal approximation of original nonlinear dynamics in each iteration[33].

$$E(q^k, u^k) = \sum_{i=1}^{N} \left\| q_{i-1}^k - q_i^k + \frac{\Delta\tau}{2}\left[f_q(q_{i-1}^k) + B(q_{i-1}^k)u_{i-1}^k + f_q(q_i^k) + B(q_i^k)u_i^k\right]\right\|_1 \quad (87)$$

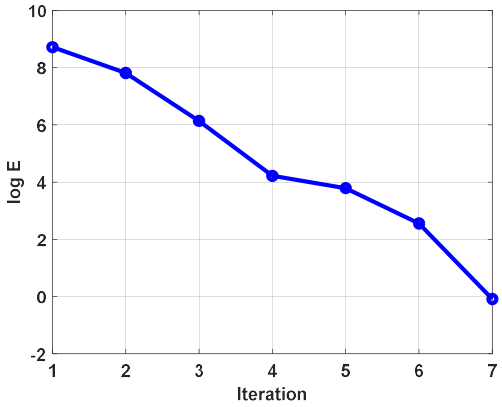

FIGURE 6. Sequential Values of Residual Function

Figure 6 shows the natural logarithm of residual function and it can be seen that residual values continuously decreasing with iteration. The following figure shows the comparison results of two control variables, u_1^2 and u_2, and shows that two values are calculated to be the same, and then lossless convexification was successfully performed as proved in Section IV.

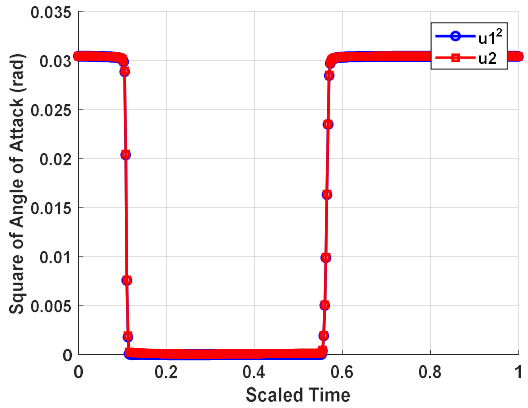

FIGURE 7. Comparison Result of Control Variable on P4 problem with $c_V = 0.0015$

b) Sequential convex programming results with $c_V = 0$

If there is no regularization term, as in the original problem, lossless convexification is not guaranteed, as explained in Section IV. In Figure 8, the results of the two control variables are not the same in some intervals in the case of the no regularization term. In this case, it is difficult to determine whether the optimization results are trustworthy.

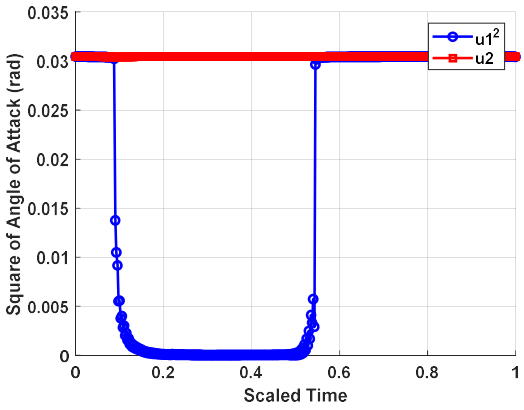

FIGURE 8. Comparison Result of Control Variable on P4 problem without regularization term ($c_V = 0$)

For practical application, the sensitivity of initial conditions or parameter settings is a very important factor. Therefore, the comparative simulation results with different initial conditions and various number of discrete sections are shown in the following. At first, the initial flight path angle in Eq. (84) is changed from 30° to 60° in 10° intervals for the sensitivity of initial condition. Figure 9 shows the converged trajectory from different initial flight path angle and it can be seen that they have quite similar profile of control variable with different transition time in Figure 10. For convergence check, sequential values of the residual function in Eq. (87) are generated in Figure 11. The number of iteration may differ depending on the initial conditions, but it can be confirmed that it shows convergent characteristics in all cases.

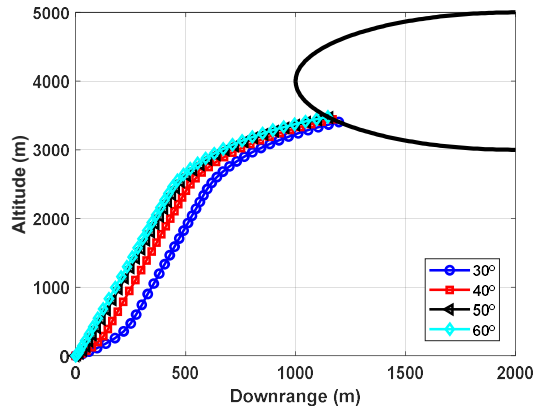

FIGURE 9. Comparison Result of Trajectory from Different Initial Flight Path Angle

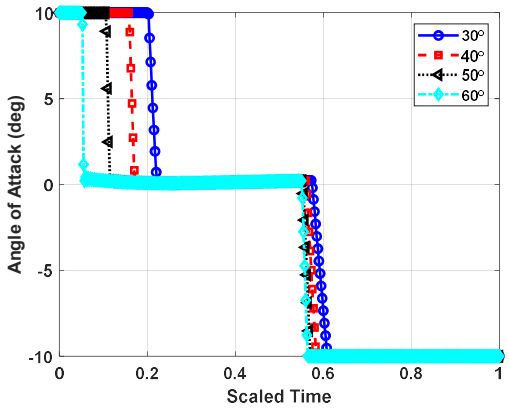

FIGURE 10. **Comparison Result of Control Variable from Different Initial Flight Path Angle**

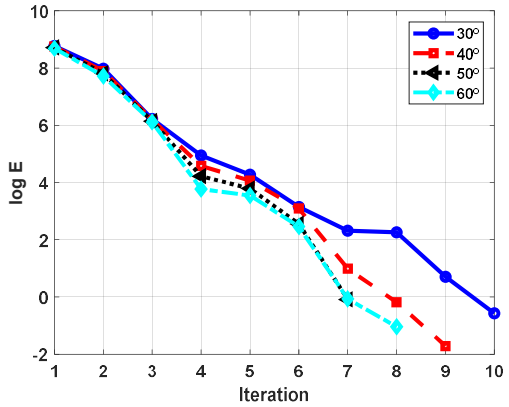

FIGURE 11. **Comparison Result of Sequential Values of Residual Function from Different Initial Flight Path Angle**

The sensitivity with respect to discrete sections is checked in Figure 12. The discrete sections are set to be from 200 to 500 in 100 intervals. Independet of the number of discrete sections, it can be seen that the convergent results are generated.

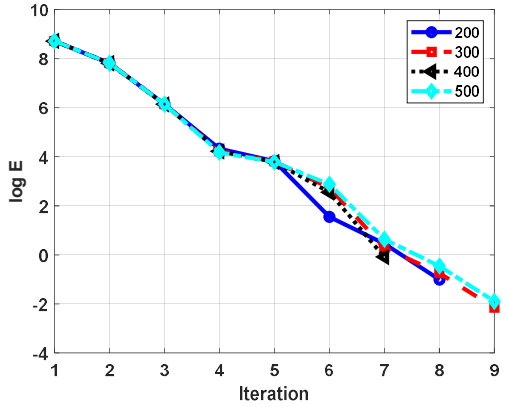

FIGURE 12. **Comparison Result of Sequential Values of Residual Function from Different Initial Flight Path Angle**

B. Comparison with Optimal Guidance Laws

In this section, the convex programming results for surface-to-air engagements are compared with the results of the widely used impact-angle-constrained optimal guidance law. In general, the optimal guidance law is designed without considering the velocity variation, corresponding acceleration limit, and flight path angle constraint. Therefore, it is difficult to generate optimal results in a realistic environment even though it provides an applicable simple analytical solution.

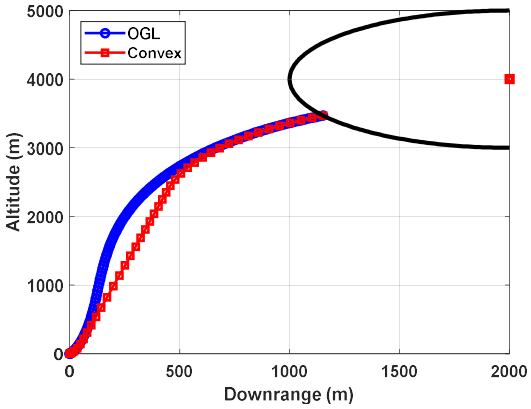

FIGURE 13. **Comparison Result of Flight Trajectory to OGL with the same Impact Angle**

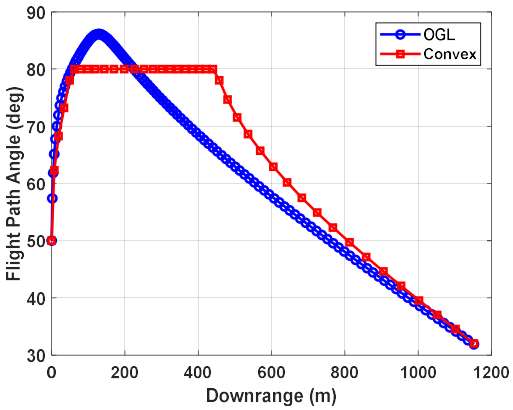

FIGURE 14. **Comparison Result of Flight Path Angle to OGL with the same Impact Angle**

The convex programming results were compared to the results of the optimal guidance law with the same impact angle constraint of 32° in Figure 13 and 14. It can be seen that the optimal guidance law yields a more curved trajectory than the convex programming trajectory, which indicates that a larger maximum flight path angle is obtained using the optimal guidance law. The maximum flight path angle of the optimal guidance law was approximately 86°, which exceeded the flight path angle constraint of 80°. Figure 15 shows the comparison results for the control variable. It shows that the convex programming generates bang-off-bang type command,

This article has been accepted for publication in IEEE Access. This is the author's version which has not been fully edited and
content may change prior to final publication. Citation information: DOI 10.1109/ACCESS.2024.3491992

while the optimal guidance law produces a continuous control command within the control limit.

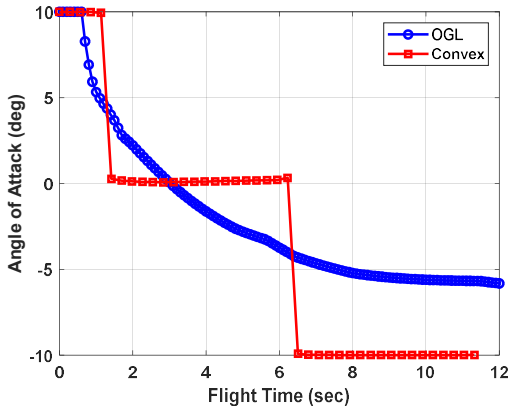

FIGURE 15. Comparison Result of Control Variable to OGL with the same Impact Angle

It can be observed that the period in which the control command is calculated as 0 is the same as the period in which the flight path angle is limited. For practical applications, the dynamics of the autopilot and predictable errors should be additionally considered in the optimization problem. Therefore, the related effect should be considered in the optimization procedure.

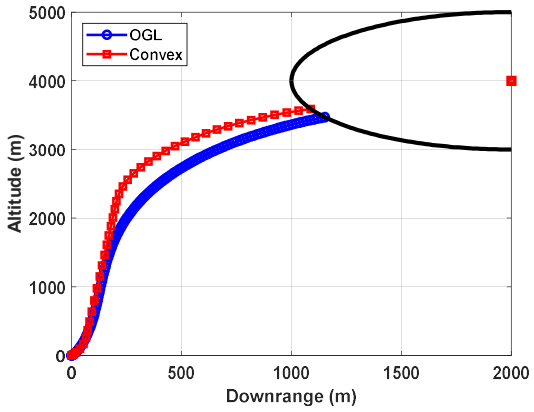

FIGURE 16. Comparison Result of Flight Trajectory to OGL with the same FPA Constraint

If the maximum flight path angle constraint of the sequential convex programming is adjusted to 86°, which is the maximum flight path angle by the optimal guidance law, the final flight path angle of the sequential convex programming is estimated to be approximately 20°. Figure 16 and 17 show flight trajectory and flight path angle with same flight path angle constraint for OGL and convex approach. This demonstrates the potential of sequential convex programming to be superior to simple analytic guidance laws in time-varying systems with constraints.

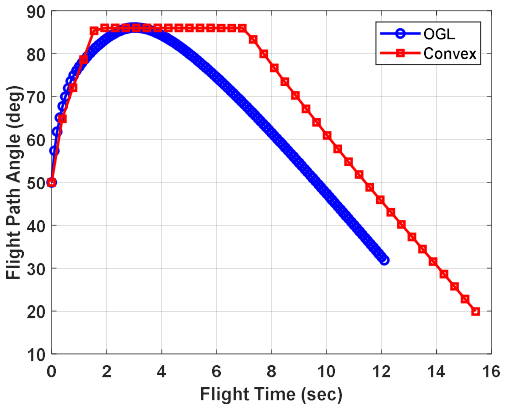

FIGURE 17. Comparison Result of Flight Path Angle to OGL with the same FPA Constraint

C. Comparison with Nonlinear Programming Results

In this section, we compare the results of sequential convex programming and those of GPOPS-II, which is a widely used nonlinear programming method for optimization.

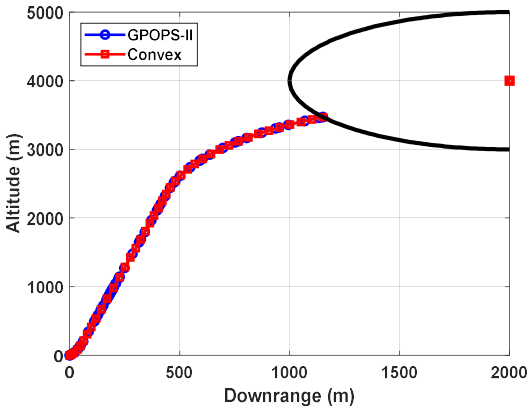

FIGURE 18. Comparison Result of Flight Trajectory to GPOPS-II

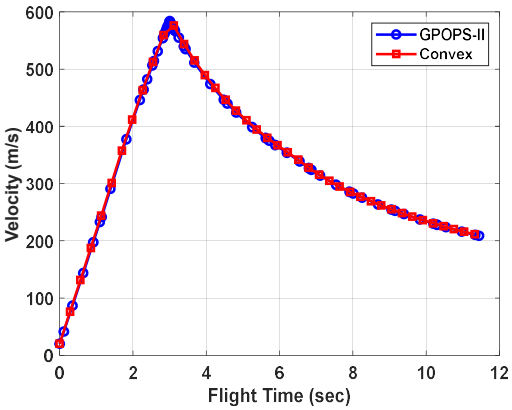

FIGURE 19. Comparison Result of Missile Velocity to GPOPS-II

The solver and tolerance of the GPOPS-II were set to IPOPT or SNOPT and 10^{-3} or 10^{-4}, respectively. The objective

function is set to be the same as that of the convex problem, including the regularization term $-c_V V(\tau_N)$. If the regularization term is not included in the objective function, the simulation results of GPOPS-II do not converge or highly oscillate, unlike convex programming, which shows convergence results that do not satisfy the control constraint. Figure 18, 19, and 20 show the comparison results for the flight trajectory, velocity, and flight path angle under the setting of INOPT and 10^{-3}, respectively. It indicates that the overall results are very similar to those of convex approach.

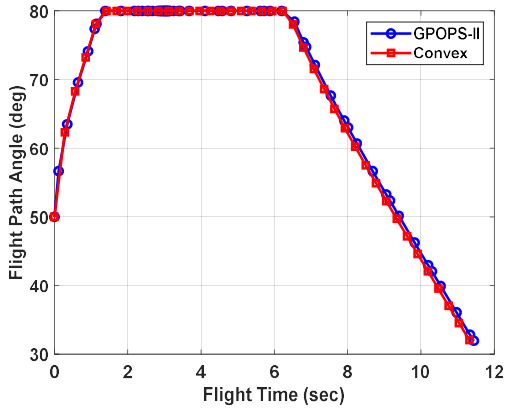

FIGURE 20. Comparison Result of Flight Path Angle to GPOPS-II

Figure 21 shows the final profile of the angle-of-attack command generated within the control limit. Although the overall result is very similar, it can be seen that slightly different results have been generated at times of abrupt command change. While convex programming produces a smoother angle-of-attack command, GPOPS-II occasionally provides a sharp result for tolerance of 1e-3.

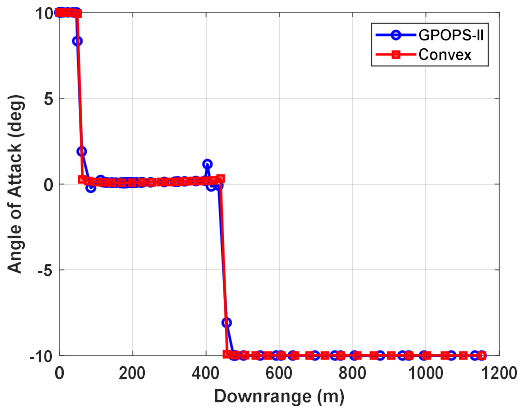

FIGURE 21. Comparison Result of Control Variable to GPOPS-II

Since this can be influenced by the tolerance and solver of GPOPS-II, the results of control variable according to the tolerance and solver in Figure 22 and Figure 23. It can be seen that as the tolerance decreases to 1e-4, smoother result is obtained, but, reducing the tolerance means that it takes more calculation time as described in Table 2. And there is also a slight, though not significant, difference depending on solvers such as IPOPT and SNOPT in this problem.

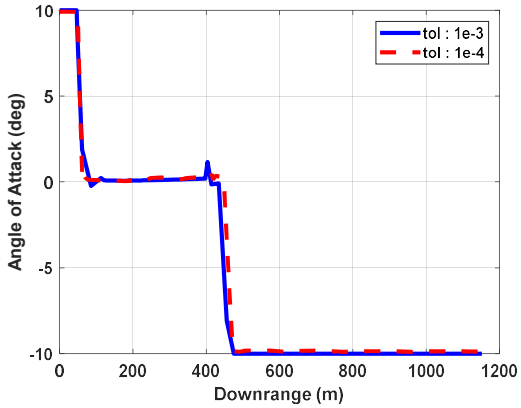

FIGURE 22. Influence of Solver with 1e-4 Tolerance of GPOPS-II

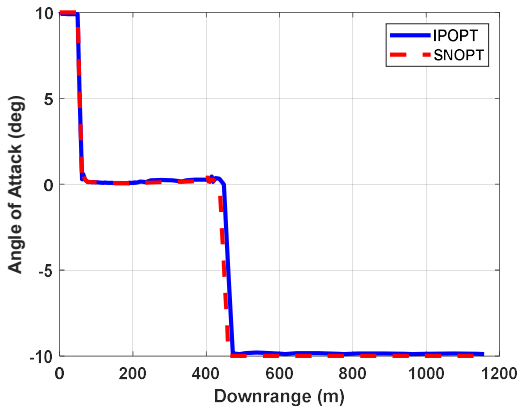

FIGURE 23. Influence of Tolerance for IPOPT solver of GPOPS-II

From the perspective of computational efficiency and applicability to real-time environment, convergence time is very crucial factor. Therefore, convergence times of convex approach and GPOPS-II are summarized in Table 2.

TABLE II
CONVERGENCE TIME OF CONVEX AND GPOPS-II APPROACH

Method	Convergence Time
Convex Approach	0.9901 sec
IPOPT with 1e-3 (GPOPS-II)	1.4086 sec
IPOPT with 1e-4 (GPOPS-II)	39.4363 sec
SNOPT with 1e-3 (GPOPS-II)	0.8540 sec
SNOPT with 1e-4 (GPOPS-II)	28.2632 sec

The results represent the average of 10 simulations, which are stably converged with small deviation in all cases. In case of convex approach, it takes less than 1 sec, whereas for GPOPS-II, there is a significant difference in computation time depending on the tolerance and solver settings. In order to achieve smooth result of control variable, a tolerance smaller than 1e-3 is required, which indicates that it takes more computation time than convex approach from Table 2. In general, nonlinear programming methods are more sensitive to initial conditions or detailed settings than convex programming for various applications. On the other hand, although the result of proposed convex approach shows more efficient than those of nonlinear programming, it seems to be rather long for real-time applications. However, it can be used effectively even if the guidance command in the mid-course guidance phase updates the optimal trajectory within tens or hundreds of milliseconds. In particular, the computation time of convex programming can be further reduced by adjusting the convergence condition, the number of discrete section, or applying customized algorithm to the individual problem. Therefore, the related research needs to be carried out to increase the possibility of practical applications.

VI. CONCLUSION

This paper provides a mid-course trajectory optimization of ground-to-air missiles for aerial defense systems based on sequential convex programming. To consider the time-varying characteristics of a solid propulsion system with state and control constraints, a convex programming approach is applied to generate the trajectory. The original nonlinear optimization problem was converted into a convex optimization problem using state augmentation, linearization of dynamics and constraints, and lossless convexification. To cope with the free final problem, the flight time was augmented to the original problem as an additional state. The nonlinear terms of the nonlinear equation and terminal constraint are linearized in convex form. For lossless convexification of the nonlinear control constraint, a modified problem is suggested using the regularization term of the final velocity and is proved based on the maximum principle. The results of the sequential convex programming show that the control constraint in the modified problem is exactly relaxed, whereas this is not the case for the original problem. It was also shown that the convex approach is more stable and robust to the initial conditions and state and control constraints with computational efficiency. Finally, the results of the analytic impact angle guidance law and nonlinear programming approaches were considered for comparison with the proposed approach. In conclusion, the proposed convex approach presents a method for stable and robust optimization to maximize the engagement area in a time-varying system with various constraints.

APPENDIX

From the optimal control theory, the Hamiltonian, the Lagrangian, and the endpoint function are defined as follows [30,35] :

$$H(t) = p_0 l(t) + p^T(t) f(t) \tag{A.1}$$

$$L(t) = H(t) + \lambda^T(t) g(t) + \nu(t) h(t) \tag{A.2}$$

$$G(t_f) = p_0 \varphi(t_f) + \xi^T(t) b(t_f) + \zeta^T(t) h(t_f) \tag{A.3}$$

where $l(t)$ and $\varphi(t_f)$ represent the Lagrangian term for running cost and Mayer term for terminal cost, respectively. And $p(t)$ is the costate variable, and λ, ν, ξ, ζ are multipliers. The following theorem represents the maximum principle with state constraints[30,35].

Theorem. Let $\{x(\cdot), u(\cdot)\}$ be an optimal pair on the interval $[t_0, t_f]$ such that $x(\cdot)$ has a finite number of junction times. Then there exist a constant $p_0 \leq 0$,, a piecewise absolutely continuous $p(\cdot)$, piecewise continuous $\lambda(\cdot)$ and $\nu(\cdot)$, a vector $\eta(i)$ for each point of discontinuity i in $p(\cdot)$, and costate ξ and ζ such that the following conditions are satisfied.

(i) the non-triviality condition

$$(p_0, p(t), \lambda(t), \nu(t), \xi, \zeta, \eta(\tau_1), \dots) \neq 0 \tag{A.4}$$

(ii) the pointwise maximum condition

$$u(t) = arg\ max\ H(t, x(t), \omega, p(t), p_0)\ \ a.e.t\ \ \omega \in \Omega(t) \tag{A.5}$$

(iii) the differential equation

$$\dot{x}(t) = \partial_p L(t) \tag{A.6}$$

$$-\dot{p}(t) = \partial_x L(t)\ \ a.e.t \tag{A.7}$$

$$\dot{H}(t) = \partial_t L(t) \tag{A.8}$$

(iv) the stationary condition

$$\partial_u L(t) = 0\ \ a.e.t \tag{A.9}$$

(v) the complementary slackness condition

$$g(t) \leq 0, \lambda(t) \leq 0, \lambda^T(t) g(t) = 0\ \ a.e.\ t \tag{A.10}$$

$$h(t) \leq 0, \nu(t) \leq 0, \nu^T(t) h(t) = 0\ \ a.e.\ t \tag{A.11}$$

$$h(\tau_i) \leq 0, \eta(\tau_i) \leq 0, \eta^T(\tau_i) h(\tau_i) = 0\ \ \forall \tau_i \tag{A.12}$$

$$h(t_f) \leq 0, \zeta \leq 0, \zeta^T h(t_f) = 0 \tag{A.13}$$

(vi) the jump condition

$$p^T(\tau_i^-) = p^T(\tau_i^+) + \eta^T(\tau_i)\partial_x h(\tau_i) \quad \forall \tau_i \tag{A.14}$$

$$H^T(\tau_i^-) = H^T(\tau_i^+) - \eta^T(\tau_i)\partial_t h(\tau_i) \quad \forall \tau_i \tag{A.15}$$

(vii) the prescribed boundary condition

$$x(t_0) = x_0, b(t_f) = 0 \tag{A.16}$$

(viii) the transversality condition

$$p^T(t_f) = \partial_x G(t_f) \tag{A.17}$$

$$-H^T(t_f) = \partial_t G(t_f) \tag{A.18}$$

REFERENCES

[1] M. Voskuijl, T. Dekkers, and R. Savelsberg, "Flight Performance Analysis of the Samad Attack Drones Operated by Houthi Armed Forces," Science & Global Security, vol. 28, issue 3, 2020.
[2] T. Shima, "Intercept-Angle Guidance," Journal of Guidance, Control, and Dynamics, vol. 34, no. 2, 2011.
[3] T. Shima, and O. M. Golan, "Head Pursuit Guidance," Journal of Guidance, Control, and Dynamics, vol. 30, no. 5, 2007.
[4] B. Kim, Y. W. Kim, N. Cho, and C. H. Lee, "Collision-Geometry-Based Optimal Guidance for High-Speed Target," Aerospace Science and Technology, vol. 115, 2021.
[5] W. Li, Y. Zhu, and D. Zhao, "Missile Guidance with Assisted Deep Reinforcement Learning for Head-On Interception of Maneuvering Target," Complex & Intelligent Systems, vol. 8, pp. 1205-1216, 2022.
[6] C. K. Ryoo, H. Cho, and M. J. Tahk, "Optimal Guidance Law with Terminal Impact Angle," Journal of Guidance, Control, and Dynamics, vol. 28, no. 4, pp. 724-732, 2005.
[7] C. K. Ryoo, H. Cho, and M. J. Tahk, "Time-to-go Weighted Optimal Guidance Law with Terminal Impact Angle Constraints," IEEE Transaction on Control System Technology, vol. 14, no. 3, pp. 483-492, 2006.
[8] B. K. Park, T. H. Kim, and M. J. Tahk, "Optimal Impact Angle Control Guidance Law Considering the Seeker's Field-of-View Limits," Journal Proceedings of the Institution of Mechanical Engineers, Part G: Journal of Aerospace Engineering, vol. 227, no. 8, pp. 1347-1364, 2013.
[9] K. S. Erer, and O. Merttopcuoglu, "Indirect Impact-Angle-Control Against Stationary Targets Using Biased Pure Proportional Navigation," Journal of Guidance, Control, and Dynamics, vol. 35, no. 2, pp. 700-703, 2012.
[10] T. H. Kim, B. K. Park, and M. J. Tahk, "Bias-Shaping Method for Biased Proportional Navigation with Terminal-Angle Constraint," Journal of Guidance, Control, and Dynamics, vol. 36, no. 6, pp. 1810-1816, 2013.
[11] R. Tekin, and K. S. Erer, "Switched-Gain Guidance for Impact Angle Control Under Physical Constraints," Journal of Guidance, Control, and Dynamics, vol. 38, no. 2, pp. 205-216, 2015.
[12] C. R. Hagraves, and S. W. Paris, "Direct Trajectory Optimization Using Nonlinear Programming and Collocation," Journal of Guidance, Control, and Dynamics, vol. 10, no. 4, pp. 338-342, 1987.
[13] D. G. Hull, "Conversion of Optimal Control Problems into Parameter Optimization Problems," Journal of Guidance, Control, and Dynamics, vol. 20, no. 1, pp. 57-60, 1997.
[14] J. T. Betts, "Survey of Numerical Methods for Trajectory Optimization," Journal of Guidance, Control, and Dynamics, vol. 21, no. 2, pp. 193-207, 1998.
[15] F. Fahroo, and I. M. Ross, "Direct Trajectory Optimization by a Chebyshev Pseudospectral Method," Journal of Guidance, Control, and Dynamics, vol. 25, no. 1, pp. 160-166, 2002.
[16] S. He, H-S. Shin, and A. Tsourdos, "Computational Missile Guidance : A Deep Reinforcement Learning," Journal of Aerospace Information Systems, vol. 18, no. 8, pp. 571-582, 2021.
[17] S. M. Lee, Y. J . Lee, Y. D. Kim, Y. S. Han, H. H. Kwon, and D. S. Hong, "Impact Angle Control Guidance Considering Seeker's Field-of-View Limit Based on Reinforcement Learning," Journal of Guidance, Control, and Dynamics, vol. 46, no.11, pp. 2168-2182, 2023.
[18] X. Wang, Y. Wang, X. Su, L. Wang, C. Lu, H. Peng and J. Liu, "Deep Reinforcement Learning-based Air Combat Maneuver Decision-Making : Literature Review, Implementation Tutorial and Future Direction," Artificial Intelligence Review Vol. 57, No. 1, 2024.
[19] P. Lu, and X. Liu, "Autonomous Trajectory Planning for Rendezvous and Proximity Operations by Conic Programming," Journal of Guidance, Control, and Dynamics, vol. 36, no. 2, pp. 375-389, 2013.
[20] X. Liu, and P. Lu, "Solving Nonconvex Optimal Control Problems by Convex Optimization," Journal of Guidance, Control, and Dynamics, vol. 37, no. 3, pp. 750-765, 2014.
[21] X. Liu, Z. Shen, and P. Lu, "Entry Trajectory Optimization by Second-Order Cone Programming," Journal of Guidance, Control, and Dynamics, vol. 39, no. 2, pp. 227-241, 2016.
[22] M. Szmuk, U. Eren, and A. W. Berning Jr., "Successive Convexification for 6-DoF Powered Descent Landing Guidance," AIAA Guidance, Navigation and Control Conference, AIAA SciTech Forum, Grapevine, Texas, USA, 2017.
[23] P. Lu, "Introducing Computational Guidance and Control," Journal of Guidance, Control, and Dynamics, vol. 40, no. 2, pp. 193, 2017.
[24] X. Liu, P. Lu, and B. Pan, "Survey of Convex Optimization for Aerospace Applications," Astrodynamics, vol. 1, no. 1, pp. 23-40, 2017.
[25] D. Malyuta, T. P. Reynolds, M. Szmuk, T. Lew, R. Bonalli, M. Pavone, and B. Acikmese, "Convex Optimization for Trajectory Generation : A Tutorial on Generating Dynamically Feasible Trajectories Reliably and Efficiently," IEEE Control Systems, vol. 42, no. 5, pp. 40-113, 2022.
[26] B. Acikmese, and S. R. Polen, "Convex Programming Approach to Powered Descent Guidance for Mars Landing," Journal of Guidance, Control, and Dynamics, vol. 30, no. 5, pp. 1353-1366, 2007.
[27] B. Acikmese, and L. Blackmore, "Lossless Convexification of a Class of Optimal Control Problems with Non-Convex Control Constraints," Automatica, vol. 47, no. 2, pp. 341-347, 2011.
[28] B. Acikmese, J. M. Carson III, and L. Blackmore, "Lossless Convexification of Nonconvex Control Bound and Pointing Constraints of the Soft Landing Optimal Control," IEEE Transactions on Control Systems Technology, vol. 21, no. 6, pp. 2104-2113, 2013.
[29] M. W. Harris, and B. Acikmese, "Lossless Convexification for a Class of Optimal Control Problems with Linear State Constraints," 52th IEEE Conference on Decision and Control, Florence, Italy, 2013.
[30] M. W. Harris, and B. Acikmese, "Lossless Convexification for a Class of Optimal Control Problems with Quadratic State Constraints," American Control Conference, Washington, DC, USA, 2013.
[31] X. Liu, Z. Shen, and P. Lu, "Exact Convex Relaxation for Optimal Flight of Aerodynamically Controlled Missiles," IEEE Transactions on Aerospace and Electronic Systems, vol. 52, no. 4, pp. 1881-1892, 2016.
[32] K. Zhang, S. Yang, and F. Xiong, "Rapid Ascent Trajectory Optimization for Guided Rockets via Sequential Convex Programming," Journal Proceedings of the Institution of Mechanical Engineers, Part G : Journal of Aerospace Engineering, vol. 233, issue 13, 2019.
[33] H. H. Kwon, and H. L. Choi, "A Convex Programming Approach to Mid-course Trajectory Optimization for Air-to-Ground Missiles," International Journal of Aeronautical and Space Sciences, vol. 21, no. 2, pp. 479-492, 2020.
[34] H. H. Kwon, S. M. Hong, G. H. Kim, and Y. H. Kim, "Mid-course Trajectory Optimization for Boost-Glide Missiles based on Convex Programming," Journal of Korean Society for Aeronautical and Space Sciences, vol. 49, no. 1, pp. 21-30, 2021. (in Korean)
[35] R. F. Harl, S. P. Sethi, and R. G. Vickson, "A Survey of the Maximum Principles for Optimal Control Problems with State Constraints," SIAM Reviews, vol. 37, no. 2, pp. 181-218, 1995.

Hyuck-Hoon Kwon received the B.S., M.S., nd Ph.D in aerospace engineering from Korea Advanced Institute of Science and Technology (KAIST), Deajeon, South Korea, in 2002, 2005, and 2020 respectively.
In 2009, he joined the LIG Nex1 for development of precision guided missiles. His research interests include convex optimization, optimal control, guidance and autopilot design, nonlinear control, and machine learning

Jang-Seong Park a received the B.S. degree in aerospace engineering from the Inha university, Inchon, South Korea, in 2011. And M.S. degrees in aerospace engineering from Korea Advanced Institute of Science and Technology(KAIST), Daejeon, South Korea, in 2013.
In 2013, he joined the LIG Nex1 for development of precision guided missiles. His research interests include, guidance and guidance filter, convex optimization, optimal control and estimation

Jeong-Hun Kim received B.S. and Ph.D. degrees in aerospace engineering from Inha University, Incheon, Republic of Korea, in 2016 and 2021 respectively. He is currently working as Research engineer with LIG Nex1 Company Ltd., Republic of Korea. His research interests include trajectory optimization, performance analysis and guidance for guided munitions.

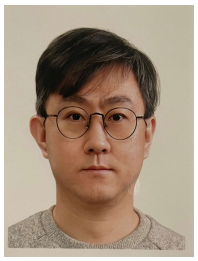

Yong-Su Han the B.S. degree in mechanical and aerospace engineering from Sejong University, Republic of Korea, in 2004, and M.S. and Ph.D. degrees in aerospace engineering from Seoul National University, Republic of Korea, in 2006 and 2012, respectively. He is currently working as a Research Fellow with LIG Nex1 Company Ltd., Republic of Korea. His research interests include performance analysis and guidance for guided munitions.